AGU ADVANCING EARTH AND SPACE SCIENCE

Water Resources Research

RESEARCH ARTICLE
10.1029/2022WR032018

Transient Storage Model Parameter Optimization Using the Simulated Annealing Method

C. H. Tsai[1,2], D. F. Rucker[1,3], S. C. Brooks[4], T. Ginn[5], and K. C. Carroll[1,2]

[1]Department of Plant & Environmental Science, New Mexico State University, Las Cruces, NM, USA, [2]Water Science and Management Program, New Mexico State University, Las Cruces, NM, USA, [3]hydroGEOPHYSICS, Inc, Tucson, AZ, USA, [4]Environmental Sciences Division, Oak Ridge National Laboratory, Oak Ridge, TN, USA, [5]Civil and Environmental Engineering, Washington State University, Pullman, WN, USA

Key Points:

- Simulated annealing with random initial guesses was able to identify correct parameter values for synthetic case with known parameter vector
- Acceptable parameter estimation (without increased iteration requirement) for Transient Storage Model (TSM) even with 5 and 10% noise was added
- Simulated annealing method was successfully applied with random initial guesses of the parameter vector for model calibration of two in-stream tracer test data sets

Correspondence to:

K. C. Carroll,
kccarr@nmsu.edu

Citation:

Tsai, C. H., Rucker, D. F., Brooks, S. C., Ginn, T., & Carroll, K. C. (2022). Transient storage model parameter optimization using the simulated annealing method. *Water Resources Research*, *58*, e2022WR032018. https://doi.org/10.1029/2022WR032018

Received 18 JAN 2022
Accepted 17 JUN 2022

Author Contributions:

Conceptualization: C. H. Tsai, D. F. Rucker, S. C. Brooks, K. C. Carroll
Data curation: C. H. Tsai, D. F. Rucker
Formal analysis: C. H. Tsai, D. F. Rucker, S. C. Brooks
Funding acquisition: C. H. Tsai, D. F. Rucker, S. C. Brooks, T. Ginn, K. C. Carroll
Investigation: C. H. Tsai, D. F. Rucker, S. C. Brooks, T. Ginn, K. C. Carroll
Methodology: C. H. Tsai, D. F. Rucker, S. C. Brooks, T. Ginn, K. C. Carroll
Project Administration: C. H. Tsai, K. C. Carroll
Resources: C. H. Tsai, D. F. Rucker, S. C. Brooks, T. Ginn, K. C. Carroll
Software: C. H. Tsai, D. F. Rucker
Supervision: C. H. Tsai, K. C. Carroll
Validation: C. H. Tsai, D. F. Rucker, S. C. Brooks, T. Ginn, K. C. Carroll
Writing – original draft: C. H. Tsai, D. F. Rucker

Abstract Hyporheic exchange in streams is critical to ecosystem functions such as nutrient cycling along river corridors, especially for slowly moving or small stream systems. The transient storage model (TSM) has been widely used for modeling of hyporheic exchange. TSM calibration, for hyporheic exchange, is typically used to estimate four parameters, including the mass exchange rate coefficient, the dispersion coefficient, stream cross-sectional area, and hyporheic zone cross-sectional area. Prior studies have raised concerns regarding the non-uniqueness of the inverse problem for the TSM, that is, the occurrence of different parameter vectors resulting in TSM solution that reproduces the observed in-stream tracer break through curve (BTC) with the same error. This leads to practical non-identifiability in determining the unknown parameter vector values even when global-optimal values exist, and the parameter optimization becomes practically non-unique. To address this problem, we applied the simulated annealing method to calibrate the TSM to BTCs, because it is less susceptible to local minima-induced non-identifiability. A hypothetical (or synthetic) tracer test data set with known parameters was developed to demonstrate the capability of the simulated annealing method to find the global minimum parameter vector, and it identified the "hypothetically-true" global minimum parameter vector even with input data that were modified with up to 10% noise without increasing the number of iterations required for convergence. The simulated annealing TSM was then calibrated using two in-stream tracer tests conducted in East Fork Poplar Creek, Tennessee. Simulated annealing was determined to be appropriate for quantifying the TSM parameter vector because of its search capability for the global minimum parameter vector.

Plain Language Summary Hyporheic exchange is critical for biogeochemical and ecological processes in river corridors, and in-stream tracer testing and modeling are commonly used for exchange characterization. Non-uniqueness of inverse modeling parameter estimation is a concern for the transient storage model (TSM) for hyporheic exchange as gradient-based parameter estimation methods tend to get trapped in local minima of the difference between observation and model results, which limits our ability to locate global minimum parameters that provide the closest match between model and data. We used a hypothetical (or synthetic) tracer test data set with known parameters to test simulated annealing as an alternative inverse modeling approach, which was also compared to the results of the commonly used TSM code, OTIS-P, a modified version of one-dimensional transport with inflow and storage (OTIS) code, couples the solution of the governing equation of OTIS with a nonlinear regression package (Runkel, 1998a). The simulated annealing method identified the "hypothetically-true" global minimum parameter vector even with variations in initial guesses of the parameter vector values and input observation data that were modified to include up to 10% noise to account for experimental error. The simulated annealing inverse TSM was also able to identify reasonable/comparable parameters for two tracer tests conducted in East Fork Poplar Creek, Tennessee, which suggests that simulated annealing is a reasonable approach for TSM inverse modeling.

1. Introduction

The hyporheic zone connects streams and rivers with groundwater, and it is recognized as critical for nutrient management and the proper functioning of stream ecosystems (Stegen et al., 2018), especially for slowly moving or small stream systems. Transport and transformation of many solutes, including nutrients, in stream corridors result from the interplay between biogeochemical processes and solute exchange between the stream channels and the metabolically active hyporheic zone (Clark et al., 2019; Meghdadi & Javar, 2018; Trauth et al., 2014).

Writing – review & editing: C. H. Tsai, D. F. Rucker, S. C. Brooks, T. Ginn, K. C. Carroll

In-stream tracer injection experiments are by far the most common method for estimating the degree to which hyporheic exchange occurs and for characterizing river corridor transport (Gooseff et al., 2013; Knapp & Kelleher, 2020; Ward et al., 2019). Data from such experiments intrinsically reflect the combined motion and mixing during stream transport with hyporheic exchange, which characteristically shifts tracer mass from earlier breakthrough into a pronounced tail reflecting enhanced residence times compared to that predicted by advection and dispersion alone. The tail of the tracer breakthrough curve (BTC) is generally more indicative of hyporheic exchange, which can have a more significant control over solute retention and spreading than dispersion processes in the stream even with lateral or back-eddy entrainments (Haggerty et al., 2000).

A Transient Storage Model (TSM) has been used to predict the mass transport in a stream (Bencala & Walters, 1983; Kelleher et al., 2013; Runkel, 1998b). The TSM considers three processes in the main channel, including the advection, dispersion, and storage exchange that is mainly associated with the hyporheic exchange. The conceptual model of TSM can be found in Wagner & Harvey (1997). For the dispersion process, the TSM represents the in-stream mass spreading due to diffusion and velocity variations through the longitudinal dispersion coefficient (D). The effects of storage within channel pools/eddies and within the hyporheic zone, are lumped into one storage exchange term, which is approximated via a first-order kinetic process with a mass exchange rate coefficient ($\boldsymbol{\alpha}$). In general, the effect of in-stream pools/eddies could possibly change the BTC (Briggs et al., 2010; Harvey et al., 2005; Rowiński et al., 2004; Scott et al., 2003). However, there were no pools or eddies observed at the field site where the tracer testing, described below, was conducted. The storage mass exchange for this study was only associated with the hyporheic exchange. On the other hand, the scaling and heterogeneity issues are important and effect the mass transport in natural systems (Yeh et al., 2015). The one-dimensional (1D) stream transport models, like TSM, are regarded as a relatively coarse approximation of the true 3D heterogeneous transport system. One approach used by prior researchers was to discretize the river into separate reach lengths and estimated different parameters for each reach length (McCallum et al., 2020). However, this research focuses on parameter optimization method for characterizing the stream mass transport for the TSM. Thus, the parameter vector in this research is effective parameter representing the entire transport length of the field site where the tracer test was conducted.

Values for D and $\boldsymbol{\alpha}$ are obtained by fitting a model to observed data by adjusting model parameter values, which requires solution of an inverse problem to calibrate the values of the parameter vector. This is commonly completed via the inverse approach, by iteratively minimizing the difference between the observations and model estimated values (an objective function). Theoretically, the calibrated parameters should be uniquely identifiable. However, lack of parameter identifiability is a problem common to parameter estimation for many types of environmental models, including the TSM (Beven & Binley, 1992; Kelleher et al., 2013). Research has indicated that the TSM non-identifiability is a result of equifinality in which different combinations of parameters can reproduce the observed BTCs with the same order of accuracy (Kelleher et al., 2013; Wagener et al., 2002), that is, the model includes multiple optimized parameter vector with local minima values of the objective function (Carrera & Neuman, 1986b). Local minima would be parameter vectors where the objective function value becomes lower than that of adjacent vectors, but local minima are generally larger than other values of the objective function when considering all values of function as a surface or distribution. Conversely, the global minimum would be the parameter vector where the objective function is lower than all other parameter vectors (Carrera & Neuman, 1986b).

Non-identifiability exists when more than one set of parameter values lead the model to reproduce the observed data within an allowable difference (Carrera & Neuman, 1986b; Knapp & Cirpka, 2017; Lemke et al., 2013). For example, Kelleher et al. (2013) used OTIS-P (Runkel, 1998b) to estimate the TSM parameters, and concluded the mass exchange rate coefficient was non-identifiable across all study reaches, including 10 BTCs for 100 m pulse injections along Stringer Creek Montana, USA (Kelleher et al., 2013). This illustrates the need for further study of the manner of inversion of the TSM model, which seems to be especially sensitive for hyporheic exchange modeling of tracer test data.

Parameter optimization or calibration methods, the numerical methods by which the parameter set is identified that produces a simulation that best fits the observed data, can be categorized into gradient and non-gradient types in terms of how the search method is conducted. Gradient methods march iteratively in a direction of steepest ascent/descent and include the Newton Raphson method, Gauss-Newton method (Gooseff et al., 2013; Scott et al., 2003), and Marquardt–Levenberg method (Bard, 1974). These methods tend to easily converge to

one of the local minima parameter vectors that is adjacent to the initial guesses of the parameter vector (Šimůnek & Hopmans, 2002). When a problem has many local minima, the gradient optimization methods may become trapped in a local minimum close to the initial guesses of the parameter vector, which are practically non-unique solutions of the inverse problem that depend on the initial guesses of the parameter vector. One way to address the local minima issue for the parameter optimization is to run the optimization model with different initial guesses of the parameter vector and compare the solution sets (Kelleher et al., 2013; Runkel, 2002; Wagener et al., 2002), but uncertainty in the global versus local nature of the final solution remains. The OTIS-P, a modified version of One-Dimensional Transport with Inflow and Storage (OTIS) code, couples the solution of the governing equation of OTIS with a Standard Time Series and Regressions Package (STARPAC) (Donaldson & Tryon, 1987). Using the adaptive, nonlinear least squares algorithm (Gauss-Newton method), OTIS-P has been a widely used optimization method for calibrating the parameters of the TSM (Runkel, 1998a; Wagner & Gorelick, 1986). The UCODE (a computer code for universal inverse modeling) (Poeter & Hill, 1999) uses the Gauss-Newton method, and has been used to estimate the parameters in the TSM for the conservative solute transport in a small mountain stream over combinations of five consecutive sub-reaches (Gooseff et al., 2013). In general, the gradient method has the potential to converge to the local minima.

Non-gradient methods do not search for global minimum parameter vector based on the direction of the gradient of objective function, and include the simulated annealing method (Kirkpatrick et al., 1983; Metropolis et al., 1953), Nelder and Mead simplex method (Bard, 1974), a sequential uncertainty fitting approach (Mousavi et al., 2012), and a host of different variations of genetic algorithms (Vrugt et al., 2001). Rowinski et al. (2004) used the nonlinear simplex method to estimate parameters in the transient storage model to characterize the process of the exchange of mass between the main-stream and the in-stream stagnant zones, which causes temporary storage of solute. The simulated annealing method (Kirkpatrick et al., 1983) is a stochastic global optimization model based on an analogy between optimization and physical annealing. It was first used for fitting the parameters for the equation of state for substances consisting of interacting individual molecules (Metropolis et al., 1953). The simulated annealing method has been applied to a large variety of optimization problems, including hydraulic parameter estimation (Rucker, 2011), decision making (Erana-Diaz et al., 2020; B. Li et al., 2019; Wang et al., 2019), resource allocation (Aerts & Heuvelink, 2002; X. Li & Ma, 2018), hazard assessment (Hackl et al., 2018; Hosseini et al., 2020), and GIS spatial optimization (Cruz-Chavez et al., 2020). We hypothesize that simulated annealing may be a feasible approach to determine the global minimum parameter vector for hyporheic zone modeling using the TSM.

The parameter non-uniqueness (equifinality) refers to occurrence of multiple values within the distribution surface of objective function, which are numeric depressions, like a crater depression in a surface, where the value of objective function is lower than the other nearby surrounding region in parameter space (Dewaide et al., 2016). The local optima problem (non-identifiability) refers to the occurrence of a valley shape of similar values in the distribution surface of an objective function, where one can vary the parameters without changing the value of objective function as long as one stays in the valley (Raue et al., 2009). Furthermore, there may be a combination of craters and valleys, and/or there may be multiple valleys and the valleys are not generally "linear" (straight) unless the forward model is linear. Because of fine-scale dependence of gradient methods on the optimization control parameters (such as, maximum allowable iterations resulting in a small decrease in the value of objective function before stopping), it is often difficult to tell the difference between a valley and a crater. These local minima of the objective function, as inverse solutions that are not as minimized as the global minimum, can be determined as the solution during gradient method optimization since those methods focus on continuously reducing the objective function, and once a gradient method migrates into a crater or a valley, it usually results in local and not global minimization or optimization.

The purpose of this research is to use the simulated annealing method to estimate the global minimum parameter vector that includes the mass exchange rate, dispersion coefficient, stream cross-sectional area, and hyporheic zone cross-sectional area for the TSM, under the assumption that a unique solution to the inverse TSM exists for the problem at hand. We first demonstrate the robustness and capability of the simulated annealing method for finding the global minimum parameter vector through a synthetic, hypothetical, test case with a known set of parameter values and compare the results with OTIS-P. Then, we apply simulated annealing inverse modeling method to obtain the parameter vector by comparison to BTC data from two in-stream tracer studies conducted

along an approximately 250 m reach of the East Fork Poplar Creek (EFPC), in Tennessee, USA. This work is the first study to apply simulated annealing to characterization of parameter vector of the TSM.

2. Simulation Methods

2.1. Transient Storage Model

The TSM (Bencala et al., 1990; Bencala & Walters, 1983; Runkel, 2002) simulates solute transport BTCs using a first-order kinetic mass transfer term driven by the concentration difference between pore water within streambed sediments and stream water. The TSM accounts for solute mass exchange between the surface water (i.e., mobile phase) and streambed pore water (i.e., assumed relatively immobile phase) through the commonly used two-domain, mobile-immobile, rate-limited, and mass-transfer conceptualization. The governing equations of the TSM include:

$$\frac{\partial C}{\partial t} = -\frac{Q}{A}\frac{\partial C}{\partial x} + \frac{1}{A}\frac{\partial}{\partial x}\left(AD_s\frac{\partial C}{\partial x}\right) + \alpha\left(C_s - C\right) \tag{1}$$

and

$$\frac{\partial C_s}{\partial t} = \alpha\frac{A}{A_s}\left(C - C_s\right) \tag{2}$$

where C [ML^{-3}] is the solute concentration in the stream; Q [L^3T^{-1}] is the stream discharge; A [L^2] is the stream cross-sectional area; D_s [L^2T^{-1}] is the longitudinal dispersion coefficient in the stream; C_s [ML^{-3}] is the solute concentration in the hyporheic zone; A_s [L^2] is the cross-sectional area of the hyporheic zone; α [T^{-1}] is the first-order, mass exchange rate coefficient across the hyporheic zone.

The simplicity of the TSM makes it an attractive option (Kelleher et al., 2013; Knapp & Kelleher, 2020; Runkel, 1998b, 2002; Wagner & Harvey, 1997; Wlostowski et al., 2017), and this modeling approach is commonly used to simulate tracer test BTCs with comparison to observed data often including calibration of the exchange rate coefficient and other parameters through parameter estimation (Bencala et al., 1990; Haggerty et al., 2000, 2002; Harvey et al., 2013; Kelleher et al., 2013; Runkel, 2002; Wagner & Harvey, 1997; Wlostowski et al., 2017). Typically, A, A_s, α, and D_s in Equations 1 and 2 are calibration parameters, since directly measuring these parameters can be challenging (Wagner & Harvey, 1997). While we assume this inverse TSM problem has a unique solution, it must be noted that there is evidence that the identifiability of the parameter values drops with either very high or very low exchange Damkohler number (DAI), which is a dimensionless combination of the rates of exchange between stream and storage zones, the stream-water velocity, and the stream reach length of the experiment (Wagner & Harvey, 1997).

The DAI was given by Bahr and Rubin as (Bahr & Rubin, 1987):

$$DAI = \alpha \times \left(1 + \frac{A}{A_s}\right) \times \frac{L_r}{v} \tag{3}$$

where L_r [L^2] is the length of the reach, and v $\left[LT^{-1}\right]$ is the average reach water velocity, in which:

$$v = \frac{Q}{A} \tag{4}$$

2.2. Parameter Estimation

The objective of our TSM inverse problem is to find the minimum in the difference between the measured and modeled concentration data, typically in a least squares formulation (F) by adjusting the value of one or more parameters in the TSM. The optimized parameter vector creates the minimum objective function value ($F(\boldsymbol{x})$) expressed as:

$$F(\boldsymbol{x}) = \sum_{i=1}^{N}\left(f_i(\boldsymbol{x}) - C_i\right)^2 \tag{5}$$

where $\boldsymbol{x}$ is the parameter vector, N is the number of observed data points, f_i is the fitting function, and C_i is the observed tracer concentrations from the tracer BTC. The f_i is a numerical solution for Equations 1 and 2 solved with finite difference method, including Crank-Nicolson for the time discretization, upwind scheme for the advection term, and second order central difference discretization for the dispersion term in Equation 1. The implementation of numerical solution f_i was verified with the solution of OTIS (Runkel, 1998a) with a root mean squared error (RMSE) for model to model comparison:

$$RMSE = \sqrt{\frac{\sum_{i=1}^{N} \left(f_i(\boldsymbol{x}) - f_{otis,i}(\boldsymbol{x})\right)^2}{N-1}} \tag{6}$$

where $f_{otis,i}(\boldsymbol{x})$ is the solution of OTIS.

2.3. The Simulated Annealing Method

The thermo-dynamic process of annealing in metallurgy consists of heating and cooling stages. At the heating stage, the mobility of molecules in the material is high, paths traveled are farther and broader, and the material can be formed in any shape. At the cooling stage molecular paths are shorter and narrower. When the temperature drops below the freezing point, the shape of material stays firm. Since the simulated annealing method utilizes this thermo-dynamic process to find the optimized parameter vector, the value of objective function $F(\boldsymbol{x})$ in Equation 5 is related to the energy. The higher energy, the higher difference between reproduced BTC and observed BTC. The simulated annealing method uses the probability to determine the candidate solution from current solution. The ΔF is the change of the energy (the difference) from the candidate solution to the current solution, defined as follows:

$$\Delta F = F\left(\boldsymbol{x}_{ca}\right) - F\left(\boldsymbol{x}_{cu}\right) \tag{7}$$

where $\boldsymbol{x}_{cu}$ is the parameter vector of the current solution and $\boldsymbol{x}_{ca}$ is the parameter vector of the candidate solution. When the temperature is below the freezing point, this method accepts the candidate solution as the next solution, and is restricted to the only condition that $\Delta F \leq 0$, from high energy to low energy, which is analogous to the gradient optimization methods. Thus, the simulated annealing method begins its optimization process with high temperature, and accepts the candidate solution as the next solution not only when $\Delta F \leq 0$ but also when $\Delta F > 0$ if

$$Prob(E) \sim \exp\left(-\frac{\Delta F}{T}\right) > \text{Random}\,(0,1) \tag{8}$$

where the $Prob(E)$ is the Boltzmann probability distribution (Kirkpatrick et al., 1983). T is the temperature schedule in the optimization process:

$$T = 1000 \times e^{-k_T N_{iter}} \tag{9}$$

in which k_T is control parameter (0.05 in this research), and N_{iter} is the total iteration number. Whenever $Prob(E)$ is greater than a random number between 0 and 1, the candidate solution is accepted as the next solution, even if the candidate solution has a higher energy than the current solution. At higher temperatures, the $Prob(E)$ is around 1, and any candidate solution is accepted as the solution, so that the solution searching is not restricted to local minima. The heating process allows the simulated annealing method to avoid being trapped in a local minimum, which provides this method with an improved chance to find the global minimum. As the temperature decreases, the simulated annealing method restricts the search capability to the vicinity around the current minimum. The stopping criteria of the simulated annealing method is varied and based on the problem of interest, but usually matches the expected noise level of the measurements. In general, searching for the parameter vector that fits the candidate of global minimum should occur before the freezing point. Thus, from numerical experimentation, we found the system would reach the global minimum parameter vector if $T < 20$ and the absolute difference of objective function between the candidate and current parameter vectors was smaller than 0.0001. The difference between the values of objective function from any parameter vector ($\boldsymbol{x}_I$) to the global minimum parameter vector ($\boldsymbol{x}_{min}$) was used to calculate the error, which is defined as follows:

$$\boldsymbol{E} = F\left(\boldsymbol{x}_I\right) - F\left(\boldsymbol{x}_{min}\right) \tag{10}$$

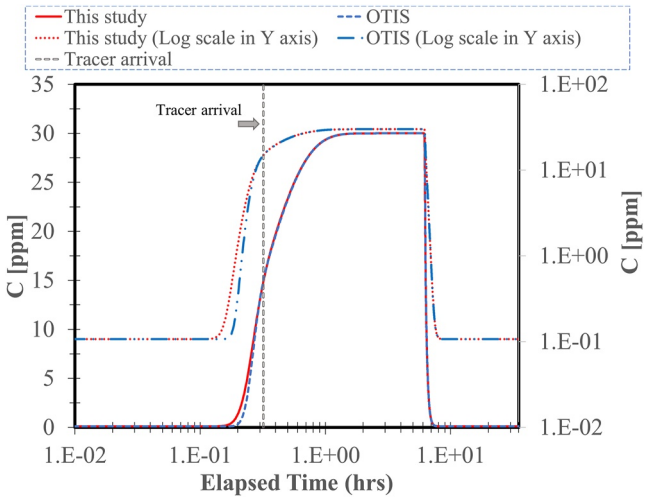

Figure 1. BTCs from our implemented TSM model to use with the simulated annealing method and results from OTIS for the synthetic test case.

Larger values of $\boldsymbol{E}$ reflect a greater deviation from the value of objective function with global minimum parameter vector. For evaluating the accuracy of the model, we again employ the RMSE calculation between the simulation and observation:

$$\overline{F} = \sqrt{\frac{\sum_{i=1}^{N} \left(f_i(\boldsymbol{x}) - C_i\right)^2}{N-1}} \tag{11}$$

The standard deviation S_j of parameter vector was calculated as follows (Carrera & Neuman, 1986a):

$$S_j = \sqrt{C_{jj}}, \qquad j = 1, 4 \tag{12}$$

where $\boldsymbol{C}_{jj}$ is the diagonal element of the parameter covariance matrix $\boldsymbol{C}$:

$$\boldsymbol{C} \approx \left(\boldsymbol{e}^T \boldsymbol{e}\right) / N \cdot \left(\boldsymbol{J}^T \boldsymbol{J}\right)^{-1} \tag{13}$$

in which the residue $\boldsymbol{e}$ is calculated as follows:

$$e_i = f_i\left(\boldsymbol{x}_{min}\right) - C_i, \qquad i = 1,\ N \tag{14}$$

the Jacobian matrix $\boldsymbol{J}$ is calculated as follows:

$$\boldsymbol{J}_{ij} = \frac{\partial\left[f_i\left(\boldsymbol{x}_{min}\right) - C_i\right]}{\partial \boldsymbol{x}_j} \tag{15}$$

The statistical analysis for the parameter vector is based on the standard deviation, S in Equation 12, with the 95% confidence interval (CI). The noise was generated by a random number generator given by:

$$s = C_i \times (1 + 2 \times (Z - 0.5) \times \sigma) \tag{16}$$

where Z: [0, 1] is given by a random number generator RANDOM_NUMBER() in Fortran 77, σ is the level of noise, that is, $\sigma = 0.05$ for 5% noise. The RANDOM_NUMBER() returns a single pseudorandom number from the uniform distribution over the range between 0 and 1.

2.4. Synthetic Test Case (Verification of Numerical Model and Capability of the Simulated Annealing Method)

To verify the correctness of the numerical solution to solve the TSM (Equations 1 and 2) for the fitting function, f_i (Equation 5), a synthetic test case was developed. To be consistent with the field tracer test described below, the tracer transport distance was 250 m, the tracer injection time for this synthetic test case was 6 hr, and the nonreactive tracer concentration peak of 30 part per million (ppm) in the stream. The stream discharge (Q) was 1 $m^3\ s^{-1}$ with stream (A) and hyporheic zone (A_s) cross-sectional areas equal to 3.8 and 2.0 m^2, respectively. Stream mass exchange rate coefficient and dispersion coefficient were set as $\alpha = 0.001\ s^{-1}$ and $D_s = 0.5\ m^2\ s^{-1}$. Figure 1 shows the BTCs from our implemented TSM (to be used with the simulated annealing method) in comparison with the results from OTIS with the same tracer arrival time (0.32 hr) The difference between the two curves was minimal except for the early-time, rising-concentration limb (0.1–0.3 hr). The RMSE was equal to 0.077, under the same spatial-temporal resolution (time step size = 0.002 hr, and spatial interval = 2 m). The mass recovery for both simulations reached 99.64%. This synthetic test case was then used to demonstrate the global search capability of the simulated annealing method for parameter estimation.

3. Field Site and Experiments

3.1. Study Area

The experimental reach is located approximately 5.4 km upstream of the mouth of EFPC, a third-order stream in the southern Appalachians in eastern Tennessee, USA (Figure 2). The site is co-located with an instrumented gauging station that provides stage, discharge, and multiparameter water quality data at 15 min intervals (Brooks

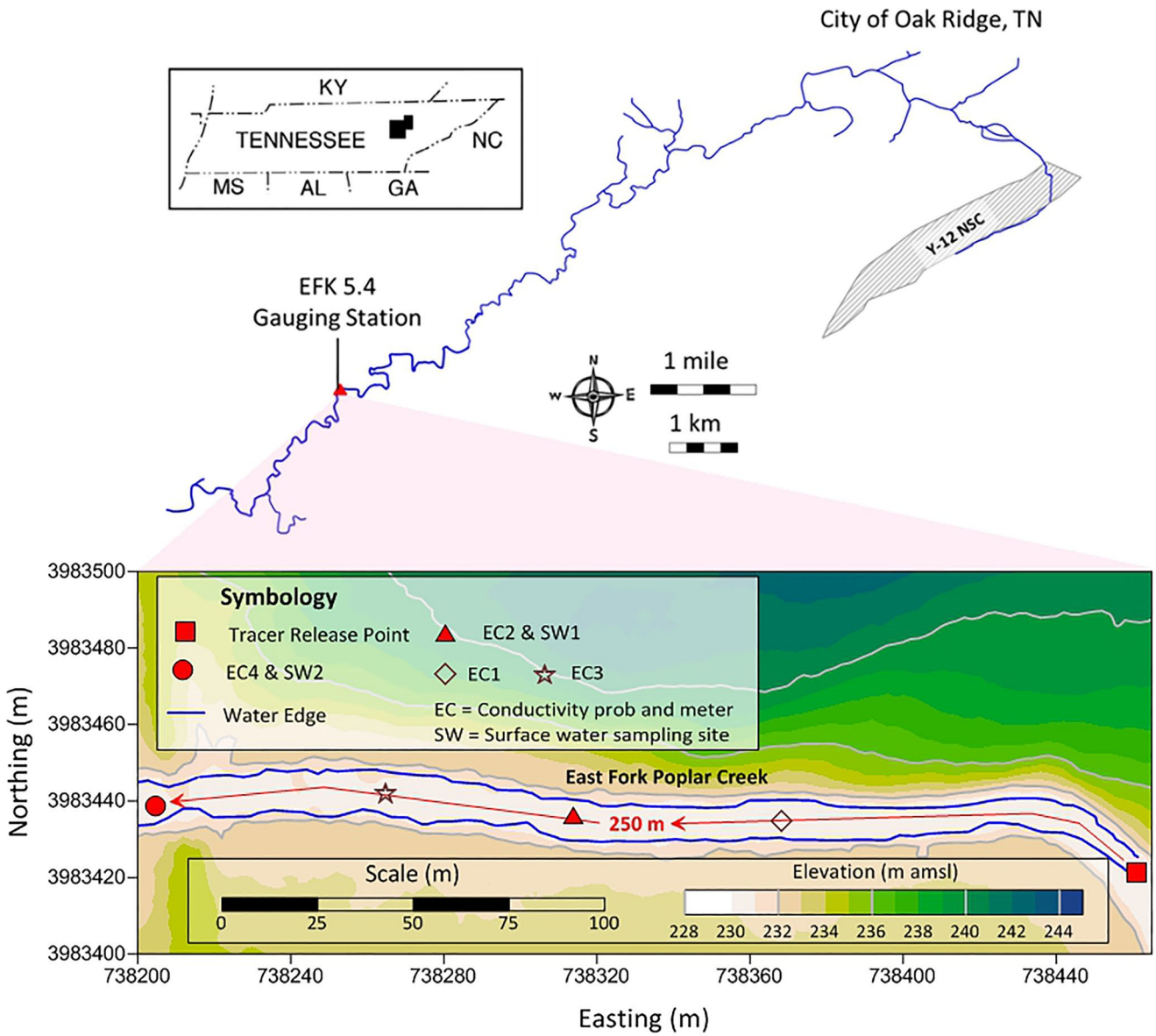

Figure 2. Study area location map illustrating the study reach location along EFPC near Oak Ridge, TN, and the tracer release and water sampling locations. The blue line indicates width of the water-filled channel.

& Lowe, 2018). The EFPC stream channel was surveyed using Leica total station TS02 (±6 mm), then a GPS (Topcon HyperLite+; ±3 mm) was used to place the local survey in Universal Transverse Mercator system.

Within the reach that the tracer tests were conducted, the stream banks consisted of natural undisturbed soils (Dickson et al., 2015) and bedrock outcrops. The streambed consisted of a relatively thin (<∼1 m) veneer of intermixed cobbles, gravel, sands, silts, and clays as well as some sections of the creek bed that are limestone bedrock (Brooks et al., 2017). Dominant vegetation along the stream in the study reach included deciduous trees typical of the area (dominantly sycamore, with some maple, and oak) and herbaceous understory. Many of the other characteristics and studies of the EFPC stream have been summarized elsewhere (Loar et al., 2011; Mohamed et al., 2021; Riscassi et al., 2016; Rucker et al., 2021).

Table 1
Three Initial Guesses of the Parameter Vector Used to Initiate the Search for the Synthetic Test Case (G1: Initial Guess 1; G2: Initial Guess 2; G3: Initial Guess 3) for Simulated Annealing and OTIS-P, and the Final Parameter Vector Returned

	Initial guess				Final result						
	α (s^{-1})	D_s (m^2 s^{-1})	A (m^2)	A_s (m^2)			α (s^{-1})	D_s (m^2 s^{-1})	A (m^2)	A_s (m^2)	$\overline{F}$ (mg L^{-1})
G1	1.16E−04	0.51	0.25	5.23	SA		1.E−03 (±3.1$E-17$)	0.5 (±4.8$E-14$)	3.8 (±4.44$E-14$)	2.0 (±2.85$E-14$)	1.29$E-14$
G2	2.42E−04	0.14	4.57	8.54	OTIS-P	G1	X	X	X	X	X
G3	1.23E−05	0.49	5.72	0.19		G2	X	X	X	X	X
						G3	9.89E−4 (±4.71$E-7$)	0.78 (56%) (±7.17$E-4$)	3.77 (±6.67$E-4$)	1.98 (±4.39$E-4$)	0.17

Note. Values in parentheses indicate the uncertainty of the parameters based on the 95% CI. The simulated annealing method reached the same parameter values for the different initial guesses of the parameter vector. SA indictates the simulated annealing method, and X indicates divergence.

3.2. Tracer Experiments

Two sodium bromide (NaBr), in-stream tracer tests were conducted on the dates of 15 January 2018 and 11 July 2018. The January test was initiated 23 days after the last daily rainfall total of 0.5 inches or greater with a base flow rate equal to 1.26 ± 0.137 m^3s^{-1}. The July test was initiated 4 days after the most recent daily rainfall total of 0.5 inches or greater with a base flow rate equal to 0.97 ± 0.0371 m^3s^{-1}. February through December 2018 were wetter than average presenting challenges in finding a window of opportunity to conduct the tracer test. Prior to initiating each test, the surface water monitoring station was established 250 m downstream of the tracer injection location (Figure 2), where samples were collected at the center of the stream. An additional sampling and monitoring station was established upstream of the injection location to quantify any changes in upstream boundary conditions during each test. Sampling began prior to the start of each test to quantify baseline values, which were subsequently used to judge when tracer arrived and had passed by the monitoring location.

The injection solution was prepared by dissolving NaBr in EFPC water in several 0.114 m^3 (30 gallon) containers. Samples of the injection solutions were collected for analysis. The tracer was introduced to the stream using a peristaltic pump for 6 hr to ensure plateau concentrations were achieved at the farthest downstream monitoring location. Water samples were collected using one of two methods. The first method involved manually sampling in the creek by triple rinsing the barrel of a 25 mL polypropylene syringe with creek water then filling the syringe with water. The second method involved sampling from the creek bank using a submersible pump whose intake was located approximately mid-depth in the water column. All samples were filtered in the field (0.2 μm polyethersulfone syringe filters), and held in a cooler in the field until return to the laboratory where they were refrigerated until bromide analysis by ion chromatography (U.S. EPA, 1997). Quality assurance/quality control included collecting duplicate field samples, field and lab blanks, and replicate analyses in the lab. The lower detection limit for the bromide analysis was 0.0048 mgL^{-1} or ppm.

4. Results and Discussion

4.1. Synthetic Test Case

We used the synthetic prediction results as the input for the inverse model to test the simulated annealing method for parameter estimation. Three initial guesses of the parameter vector, randomly generated, were used to test the capability of simulated annealing parameter optimization for finding the parameter vector that returns the global minimum value of the objective function starting from a range of differing initial guesses of the parameter vector (Table 1). The initial parameter estimates were randomly given by the RAND () function in EXCEL in OFFICE 365 with $\alpha : \left[10^{-6}, 10^{-3}\right)$, $D_s : [0.01, 2)$, $A : [10^{-3}, 9.999)$, $A_s : [10^{-3}, 9.999)$ through linear mathematical projection. For this first test case, no noise was added to the input data.

The simulated annealing method converged after 67 iterations with a resulting RMSE, $\overline{F}$, of 1.29E−14 ppm, which would be considered negligible. For each of the three different initial guesses of the parameter vector, the a priori-assigned correct parameter vector was determined by the simulated annealing method (Table 1). This result

Table 2
The Results From the Simulated Annealing Method and OTIS-P for the Data Set With the Level of Noise Equal to 5% and 10% (G1: Initial Guess 1; G2: Initial Guess 2; G3: Initial Guess 3)

Noise			α (s^{-1})	D_s (m^2 s^{-1})	A (m^2)	A_s (m^2)	$\overline{F}$ (mg L^{-1})
5%	SA		1.00E−03 (±2.4$E-04$)	0.5 (±0.371)	3.80 (±0.34)	2.00 (±0.22)	0.14
	OTIS-P	G1	X	X	X	X	X
		G2	X	X	X	X	X
		G3	9.88E−04 (±2.27$E-3$)	0.79 (58%) (±3.48)	3.77 (±3.23)	1.97 (±2.12)	0.23
10%	SA		9.94E−04 (±4.68$E-04$)	0.495 (±0.58)	3.79 (±0.61)	1.97 (±0.41)	0.22
	OTIS-P		X	X	X	X	X

Note. Values in parentheses indicate the uncertainty of the parameters based on the 95% CI. The simulated annealing method reached the same parameter for the different initial guesses of the parameter vector. SA indictates the simulated annealing method, and X indicates divergence.

confirms that the simulated annealing method was capable of identifying the global minimum parameter vector for noise-free synthetic data under a variety of different and randomly generated initial guesses of the parameter vector. The OTIS-P converged on the third initial guesses of the parameter vector, but failed to converge for the first two. The relative difference of parameter D_s from the correct to the estimated parameter was up to 56% $\left(\frac{(0.78-0.5)}{0.5} \times 100\% = 56\%\right)$ when OTIS-P was used.

Next, we modified the simulated BTC data to create two noisy data sets using Equation 16 (5–10% noise applied to input observation data was considered a reasonable amount of experimental error). For the BTC that included 5% noise, simulated annealing method recovered the parameter vector that were used to generate the BTC data starting with each of the three initial guesses, while the OTIS-P converged only on the third guess (Table 2). As the noise level went up to 10%, the simulated annealing method still succeeded in finding the correct parameters with only minor error, while OTIS-P failed to converge for three initial guesses of the parameter vector. This demonstrates the capability of the simulated annealing method for finding the global minimum parameter vector even with uncertainty and variability in the observation data inputs.

In terms of accuracy, the inclusion of the noise increased the level of difference between the simulated and observed BTCs. The RMSE increased from 10^{-14} with no noise added to 0.142 and 0.224 with 5% and 10% noise added, respectively. There was negligible deviation from the correct parameter vector for the 5% noise case, but for the 10% noise case the relative difference from the correct parameter A_s was 1.5% $\left(\frac{(2-1.97)}{2} \times 100\% = 1.5\%\right)$. Similarly, the relative difference from the correct parameters was 0.6, 1, and 0.26 for α, D_s, and A, respectively. These differences from the correct parameter vector increased with increasing noise level, especially for the A_s that varied by 1.5% for the data containing 10% of noise. For OTIS-P, the relative difference from the correct parameter D_s had increases up to 58%.

Computational efficiency is an important factor for an optimization method, because the number of iterations, and computer simulation time, needed to optimize the parameter estimation can be significant. Table 3 shows a comparison of number of iterations required for convergence using simulated annealing with the synthetic BTC data containing different levels of noise as input. The simulated annealing method converged within a similar number of iterations (i.e., between 61 and 67 iterations) regardless of the noise level. These results support the versatility of the simulated annealing method application for TSM parameter estimation. Overall, the results with

Table 3
The Numbers of Iterations for the Simulated Annealing Method Scenarios With Different Initial Parameter Vectors and Amounts of Noise Added to the Data

	Noise-free			5% noise			10% noise		
	G1	G2	G3	G1	G2	G3	G1	G2	G3
Simulated annealing method	67	62	65	62	61	61	62	63	63

Note. G1: Initial Guess 1, G2: Initial Guess 2, G3: Initial Guess 3.

the synthetic test case demonstrated the robustness of the simulated annealing method for parameter estimation and supported the applicability of this method for hyporheic zone exchange modeling.

The parameter variation paths for iterations starting with the initial guesses of the parameter vector and ending with the global minimum parameter vector for the synthetic test case are shown in Figure 3. Multiple parameters were changed in each iteration, and parameter values both increased and decreased in value along the path. For the four values in the parameter vector, all of the search paths eventually reached the same parameter values where the global minimum parameter vector was located. Because the searching direction of the simulated annealing is randomly determined, there is no specific route the simulated annealing method uses to find the $\boldsymbol{x}_{min}$.

The difference between the values of objective function (Equation 9) for each parameter vector for each search iteration is plotted in Figure 4. With each of the three different initial guesses of the parameter vector, the difference as described by the measure **E** (Equation 10) decreased approximately 10 orders of magnitude from $10^{1.5}$ to 10^{-9} during the optimization process. Also, **E** was initially fluctuating with both increases and decreases in values, illustrating the ability of the simulated annealing method to potentially escape local minima in its search for the global minimum parameter vector. The results from Figures 3 and 4 demonstrate the capability of the simulated annealing method to find the global minimum parameter vector for the TSM without getting trapped in local minima as can happen with gradient methods.

4.2. Modeling Field-Site Tracer Test BTCs From EFPC

The simulated annealing method was used to acquire the optimized parameter vector using input data measured with samples collected during the field tracer tests conducted in the EFPC. Three randomly generated initial guesses of the parameter vector were used to start the parameter optimization of TSM in comparison to both of the tracer tests conducted in the EFPC (Table 4). It is noted that the initial guesses of the parameter vector were randomly given by the RAND () in EXCEL in OFFICE 365 with $\alpha : \left[10^{-6}, 10^{-3}\right)$, $D_s : [0.01, 2)$, $A : [10^{-3}, 9.999)$, $A_s : [10^{-3}, 9.999)$.

The simulated annealing method converged to the same final parameter vector for each of the three initial guesses of the parameter vector (Table 4). Because these two tracer tests were conducted at different times (January and July), the converged parameters are different from each other. The mass exchange coefficient and the dispersion coefficient in Table 4 are similar to the results published in the literature (Wagner & Harvey, 1997). The mass exchange coefficient for Test 1 ($\alpha = (4.8 \pm 0.134) \times 10^{-4} s^{-1}$) was smaller than that of Test 2 ($\alpha = (8.5 \pm 0.471) \times 10^{-4} s^{-1}$). This result may be due to the lower discharge rate during Test 2 (0.97 $m^3 s^{-1}$) compared to that of Test 1 (1.26 $m^3 s^{-1}$). Although, hyporheic zone exchange is not solely dependent on stream discharge, and both positive and negative correlations between hyporheic exchange and stream flow have been reported in prior studies (Ward & Packman, 2019). Similarly, the dispersion coefficient, D_s, for Test 1 was smaller ($0.028 \pm 0.042\ m^2 s^{-1}$) than for Test 2 ($0.046 \pm 0.15\ m^2 s^{-1}$). We also attribute this variability in dispersion as due to the above noted differences in discharge rate and stream velocity. In addition, Test 2 had a larger hyporheic zone cross-sectional area ($A_s = 1.82 \pm 0.03\ m^2$) compared to the Test 1 ($A_s = 1.60 \pm 0.015\ m^2$). The RMSE, $\overline{F}$, were 0.60 for Test 1 and 0.89 for Test 2, and the required number of iterations for the simulated annealing method ranged from 61 to 68. The value of DAI was calculated as 1.95 and 1.81 based on Equation 3. Since the value of DAI is greater than 1, the storage exchange rate is significantly greater than advective velocity, indicating the EFPC can be considered as a slowly moving stream with rapid transient storage exchange (Kelleher et al., 2013).

Comparison of the observed and calibrated simulation results of tracer test BTCs are plotted in Figure 5 with normalized concentration (sample concentration divided by the plateau in-stream concentration), versus the elapsed time after the start of tracer injection. The log (Figure 5a) and linear (Figure 5b) timescales are presented for visualization and comparison between the observed data and the results of the calibrated simulation. The two bromide tracer test BTCs were comparable, which might be expected given the similarity of the flow rate for each test (Figure 5). In each of the two tracer tests, there was a sharp increase in bromide concentration to C/C_0 of 0.5 within an average of ~0.5 hr at the downstream location (Figure 5a) after the tracer was first added to the creek. Steady concentrations then persisted for the duration of the tracer injection. The relatively constant C/C_0 values during the injection suggest that the tracer solution was mixed throughout the full volume of the EFPC along the 250 m reach.

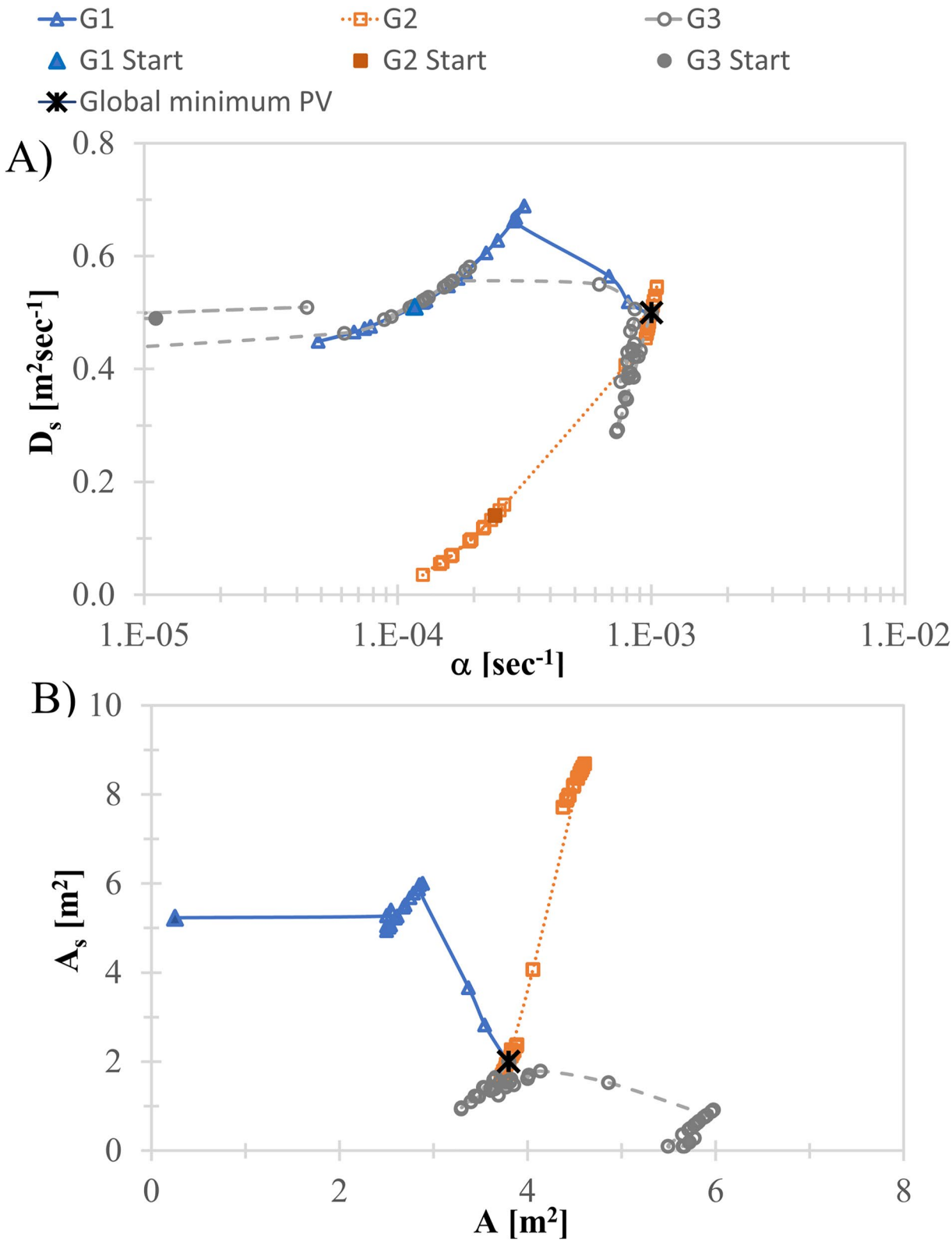

Figure 3. The paths to finding the global minimum of the objective function using simulated annealing and with different initial guesses of the parameter vectors for the noise-free synthetic test cases, (a) $\boldsymbol{\alpha}$ vs. $\boldsymbol{D}_s$, (b) A versus A_s. The solid line is the path for the G1, the short dash is for the G2, and the long dash is for the G3.

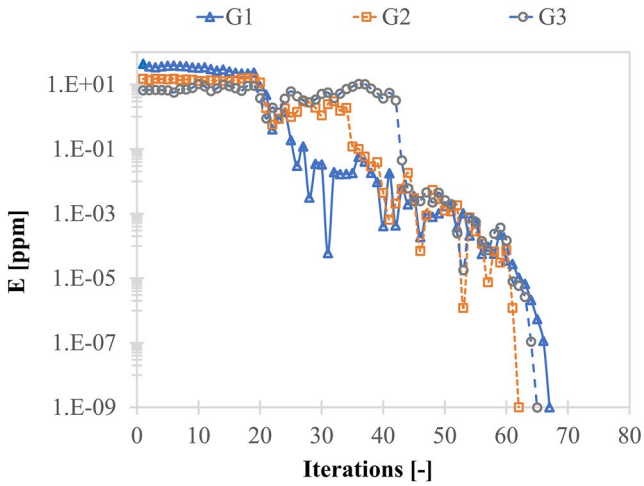

Figure 4. The parameter estimation error (difference between the values of objective function for parameter vector relative to that of the global minimum parameter vector) during simulated annealing search iterations for each of the three initial guesses of the parameter vectors.

Following cessation of tracer injection, concentrations began decreasing similar to the increasing concentration during initial tracer arrival portion of the BTC. A concentration spreading behavior and slope variation at the ascending and descending concentration limbs of the BTCs were also observed. Bromide concentrations declined rapidly then exhibited a more gradual decrease before they reached background concentrations (Figure 5b). Decreasing tracer concentration during elution was slightly delayed relative to the arrival of the tracer, and we attribute that to solute retention within the streambed sediment pore waters due to hyporheic exchange or stagnant near-bank surface water. However, the concentration tailing was relatively minor due to the relatively thin zone of unconsolidated sediments and clayey bank soils overlying the limestone bedrock at the EFPC study site (Mohamed et al., 2021; Rucker et al., 2021). The TSM simulation matched the observed data well over the full time range of each test. The simulated annealing inverse TSM determined parameter vectors that captured the rapid concentration increase, several-hours-long plateau, concentration-decrease, and concentration-tailing portions of the observed BTC.

5. Conclusions

This investigation evaluated the simulated annealing method for determining the optimal parameter vector of the TSM for simulating hyporheic exchange. The non-uniqueness problem of parameters in the optimization of the TSM has been an issue noted previously in the literature. To overcome this, we applied simulated annealing as a global estimation procedure to help overcome issues related to local minima. The capability and robustness of the simulated annealing method was examined using synthetic test cases with and without the addition of differing amounts of random noise in the input data. The results from these synthetic test cases showed the success of simulated annealing for optimizing the parameter set and determining the correct parameter vector, and the approach was confirmed to be feasible with only minor error and deviation from the correct parameters even for cases with added noise up to 10% without increased number of iterations required for convergence. This provides confidence in applying the simulated annealing method to quantify the parameter vector in the TSM for the field observed BTCs since the field data set is generally expected to include some experimental error. The simulated annealing method was also successfully applied to calibration of the parameter vector (i.e., mass exchange rate coefficient, dispersion coefficient, stream cross-sectional area, and hyporheic zone cross-sectional area) for the TSM using the BTC data measured during two tracer tests conducted in the EFPC. The calibrated parameter sets were comparable between the two tracer test data sets, and the minor differences were attributed to differences in stream flow rate between the two tracer tests. The optimization produced low RMSE values, and the simulation BTCs were highly comparable with the observations. Simulated annealing provides a robust alternative for TSM parameter estimation to avoid the commonly occurring parameter estimation constraints. As for if simulated annealing method superior to the other global optimization methods, this is a potential future research topic of interest.

Table 4
Three Initial Guesses of the Parameter Vector Used to Initiate the Search for Both Tracer Tests Conducted in the EFPC (G1: Initial Guess 1; G2: Initial Guess 2; G3: Initial Guess 3) and the Final Parameter Vector Returned

	Initial guess					Final results				
	α (s^{-1})	D_s (m^2s^{-1})	A (m^2)	A_s (m^2)		α (s^{-1})	D_s (m^2s^{-1})	A (m^2)	A_s (m^2)	$\overline{F}$ (mg L^{-1})
G1	2.35E−04	0.01	5.26	9.92	Test 1	4.8E−04 (±1.34$E-5$)	0.0283 (±0.0424)	4.98 (±0.0160)	1.60 (±0.0152)	0.60
G2	3.37E−04	0.11	6.74	3.3	Test 2	8.50E−04 (±4.71$E-5$)	0.0464 (±0.146)	3.07 (±0.0384)	1.82 (±0.0319)	0.89
G3	1.13E−05	1.01	8.23	4.05						

Note. Values in parentheses indicate the uncertainty of the parameters based on the 95% CI. It is noted that simulated annealing method reached the same parameters for the different initial guesses of the parameter vector.

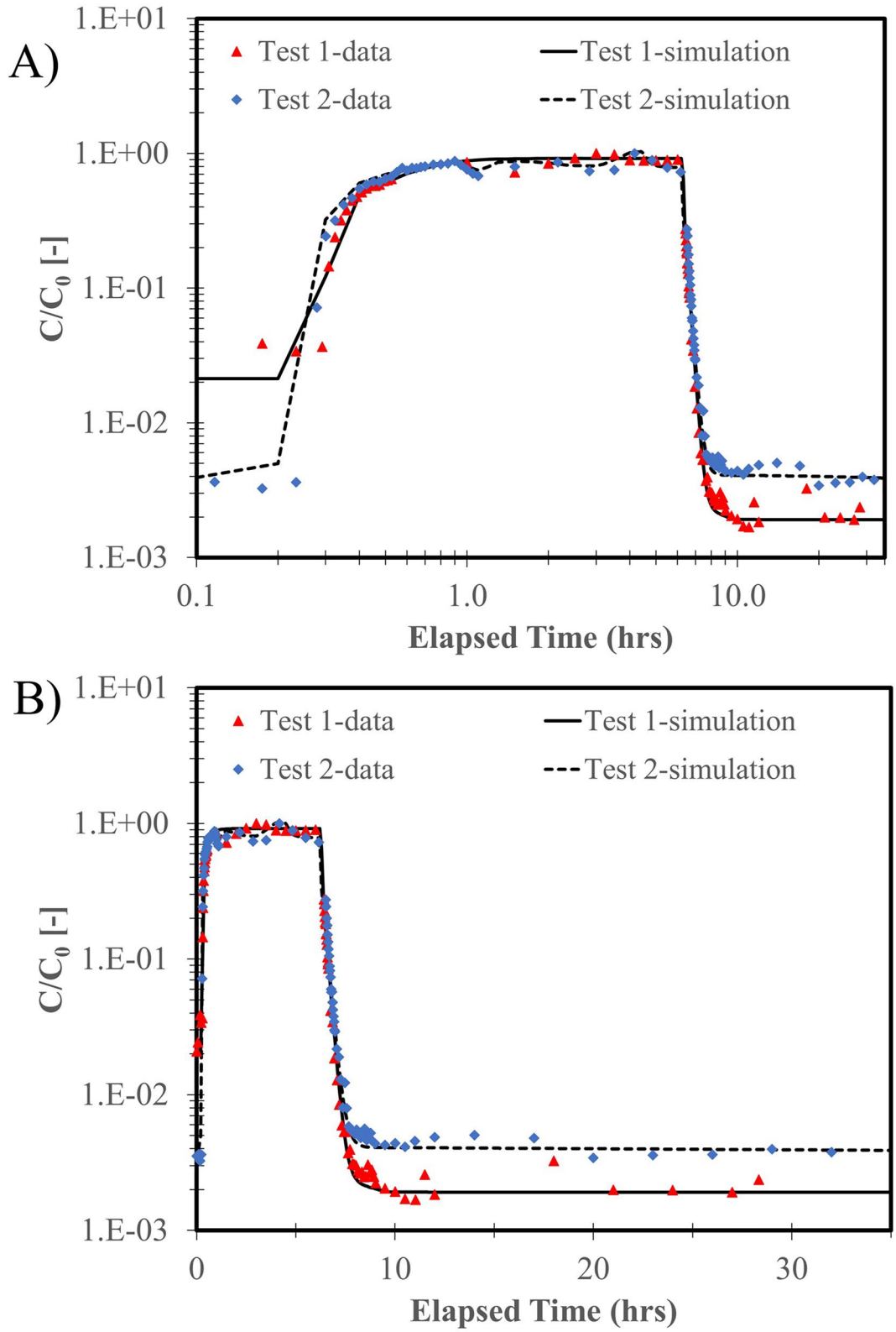

Figure 5. Measured (symbols) and simulated (lines) bromide breakthrough curves for the tracer tests conducted in EFPC presented as normalized concentration (where C is normalized by C_0 = maximum plateau concentration) vs. elapsed time since the bromide addition started (a) log-log scale, (b) semi-log scale.

Data Availability Statement

The data set (Brooks & Lowe, 2018) are freely available at https://www.esd.ornl.gov/programs/rsfa/data.shtml.

Acknowledgments
This work was supported by the Department of Energy Minority Serving Institution Partnership Program (MSIPP) managed by the Savannah River National Laboratory (0000525176). Additional support was provided by the NSF (Award Number (FAIN): 2142686), USDA National Institute of Food and Agriculture (Hatch project 1023257), NMSU Ag. Experiment Station, and the U.S. Department of Energy, Office of Science, Biological and Environmental Research, Subsurface Biogeochemical Research Program to the Science Focus Area (SFA) at ORNL. Oak Ridge National Laboratory is managed by UT-Battelle, LLC, for the U.S. Department of Energy under contract DE-AC05-00OR22725. We appreciate the assistance of Kenneth Lowe, Michael Jones, NikkiJones, Justin Milavec, Tanzila Ahmed, and Chris Kubicki. We appreciate the thoughtful and supportive comments of Associate Editor Jan Fleckenstein and the reviewers, including Julia Knapp, which improved the clarity of this work.

References

Aerts, J. C. J. H., & Heuvelink, G. B. M. (2002). Using simulated annealing for resource allocation. *International Journal of Geographical Information Science*, *16*(6), 571–587. https://doi.org/10.1080/13658810210138751

Bahr, J. M., & Rubin, J. (1987). Direct comparison of kinetic and local equilibrium formulations for solute transport affected by surface-reactions. *Water Resources Research*, *23*(3), 438–452. https://doi.org/10.1029/wr023i003p00438

Bard, Y. (1974). *Nonlinear parameter estimation*. Academic Press.

Bencala, K. E., Mcknight, D. M., & Zellweger, G. W. (1990). Characterization of transport in an acidic and metal-rich mountain stream based on a lithium tracer injection and simulations of transient storage. *Water Resources Research*, *26*(5), 989–1000. https://doi.org/10.1029/wr026i005p00989

Bencala, K. E., & Walters, R. A. (1983). Simulation of solute transport in a mountain pool-and-riffle stream: A transient storage model. *Water Resources Research*, *19*(3), 718–724. https://doi.org/10.1029/wr019i003p00718

Beven, K., & Binley, A. (1992). The future of distributed models: Model calibration and uncertainty prediction. *Hydrological Processes*, *6*(3), 279–298. https://doi.org/10.1002/hyp.3360060305

Briggs, M. A., Gooseff, M. N., Peterson, B. J., Morkeski, K., Wollheim, W. M., & Hopkinson, C. S. (2010). Surface and hyporheic transient storage dynamics throughout a coastal stream network. *Water Resources Research*, *46*(6). https://doi.org/10.1029/2009wr008222

Brooks, S. C., Eller, V., Dickson, J. O., Earles, J., Lowe, K., & Mehlhorn, T. (2017). *Mercury content of sediments in east fork poplar creek: Current assessment and past trends*. Oak Ridge National Laboratory. Retrieved from ORNL/TM-2016/578 https://doi.org/10.2172/1338545

Brooks, S. C., & Lowe, K. A. (2018). East fork poplar creek discharge at kilometer 5.4 water year 2018. [Dataset] https://doi.org/10.12769/1489832

Carrera, J., & Neuman, S. P. (1986a). Estimation of aquifer parameters under transient and steady-state conditions. 1. Maximum likelihood method incorporating prior information. *Water Resources Research*, *22*(2), 199–210. https://doi.org/10.1029/wr022i002p00199

Carrera, J., & Neuman, S. P. (1986b). Estimation of Aquifer parameters under transient and steady-state conditions. 2. Uniqueness, stability, and solution algorithms. *Water Resources Research*, *22*(2), 211–227. https://doi.org/10.1029/wr022i002p00211

Clark, J. J., Qian, Q., Voller, V. R., & Stefan, H. G. (2019). Hyporheic exchange in a gravel bed flume with and without traveling surface waves. *Advances in Water Resources*, *123*, 120–133. https://doi.org/10.1016/j.advwatres.2018.11.005

Cruz-Chavez, M. A., Moreno-Bernal, P., Rivera-Lopez, R., Avila-Melgar, E. Y., Martinez-Bahena, B., & Cruz-Rosales, M. H. (2020). GIS spatial optimization for corridor alignment using simulated annealing. *Applied Sciences-Basel*, *10*(18), 6190. https://doi.org/10.3390/app10186190

Dewaide, L., Bonniver, I., Rochez, G., & Hallet, V. (2016). Solute transport in heterogeneous karst systems: Dimensioning and estimation of the transport parameters via multi-sampling tracer-tests modelling using the OTIS (one-dimensional transport with inflow and storage) program. *Journal of Hydrology*, *534*, 567–578. https://doi.org/10.1016/j.jhydrol.2016.01.049

Dickson, J., Mayes, M., Earles, J., Mehlhorn, T., Lowe, K., Peterson, M., & Pierce, E. (2015). Soil investigation of lower east fork poplar creek. https://doi.org/10.2172/1352740

Donaldson, J., & Tryon, P. (1987). *User's guide to STARPAC: The standard time series and regression package: Version 2.07*. Sci. Comput. Div., Natl. Cent. for Atmos. Res.

Erana-Diaz, M. L., Cruz-Chavez, M. A., Rivera-Lopez, R., Martinez-Bahena, B., Avila-Melgar, E. Y., & Cruz-Rosales, M. H. (2020). Optimization for risk decision-making through simulated annealing. *IEEE Access*, *8*, 117063–117079. https://doi.org/10.1109/access.2020.3005084

Gooseff, M. N., Briggs, M. A., Bencala, K. E., McGlynn, B. L., & Scott, D. T. (2013). Do transient storage parameters directly scale in longer, combined stream reaches? Reach length dependence of transient storage interpretations. *Journal of Hydrology*, *483*, 16–25. https://doi.org/10.1016/j.jhydrol.2012.12.046

Hackl, J., Adey, B. T., & Lethanh, N. (2018). Determination of near-optimal restoration programs for transportation networks following natural hazard events using simulated annealing. *Computer-Aided Civil and Infrastructure Engineering*, *33*(8), 618–637. https://doi.org/10.1111/mice.12346

Haggerty, R., McKenna, S. A., & Meigs, L. C. (2000). On the late-time behavior of tracer test breakthrough curves. *Water Resources Research*, *36*(12), 3467–3479. https://doi.org/10.1029/2000wr900214

Haggerty, R., Wondzell, S. M., & Johnson, M. A. (2002). Power-law residence time distribution in the hyporheic zone of a 2nd-order mountain stream. *Geophysical Research Letters*, *29*(13), 1640. https://doi.org/10.1029/2002gl014743

Harvey, J. W., Bohlke, J. K., Voytek, M. A., Scott, D., & Tobias, C. R. (2013). Hyporheic zone denitrification: Controls on effective reaction depth and contribution to whole-stream mass balance. *Water Resources Research*, *49*(10), 6298–6316. https://doi.org/10.1002/wrcr.20492

Harvey, J. W., Saiers, J. E., & Newlin, J. T. (2005). Solute transport and storage mechanisms in wetlands of the Everglades, South Florida. *Water Resources Research*, *41*(5). https://doi.org/10.1029/2004wr003507

Hosseini, F. S., Choubin, B., Mosavi, A., Nabipour, N., Shamshirband, S., Darabi, H., & Haghighi, A. T. (2020). Flash-flood hazard assessment using ensembles and Bayesian-based machine learning models: Application of the simulated annealing feature selection method. *Science of the Total Environment*, 711. https://doi.org/10.1016/j.scitotenv.2019.135161

Kelleher, C., Wagener, T., McGlynn, B., Ward, A. S., Gooseff, M. N., & Payn, R. A. (2013). Identifiability of transient storage model parameters along a mountain stream. *Water Resources Research*, *49*(9), 5290–5306. https://doi.org/10.1002/wrcr.20413

Kirkpatrick, S., Gelatt, C. D., & Vecchi, M. P. (1983). Optimization by simulated annealing. *Science*, *220*(4598), 671–680. https://doi.org/10.1126/science.220.4598.671

Knapp, J. L. A., & Cirpka, O. A. (2017). Determination of hyporheic travel time distributions and other parameters from concurrent conservative and reactive tracer tests by local-in-global optimization. *Water Resources Research*, *53*(6), 4984–5001. https://doi.org/10.1002/2017wr020734

Knapp, J. L. A., & Kelleher, C. (2020). A perspective on the future of transient storage modeling: Let's stop chasing our tails. *Water Resources Research*, *56*(3), e2019WR026257. https://doi.org/10.1029/2019wr026257

Lemke, D., Liao, Z., Wöhling, T., Osenbrück, K., & Cirpka, O. A. (2013). Concurrent conservative and reactive tracer tests in a stream undergoing hyporheic exchange. *Water Resources Research*, *49*(5), 3024–3037. https://doi.org/10.1002/wrcr.20277

Li, B., Yang, X. Y., & Xuan, H. (2019). A hybrid simulated annealing heuristic for multistage heterogeneous fleet scheduling with fleet sizing decisions. *Journal of Advanced Transportation*, 1–19. https://doi.org/10.1155/2019/5364201

Li, X., & Ma, X. D. (2018). An improved simulated annealing algorithm for interactive multi-objective land resource spatial allocation. *Ecological Complexity*, *36*, 184–195. https://doi.org/10.1016/j.ecocom.2018.08.008

Loar, J. M., Stewart, A. J., & Smith, J. G. (2011). Twenty-five years of ecological recovery of east fork poplar creek: Review of environmental problems and remedial actions. *Environmental Management*, *47*(6), 1010–1020. https://doi.org/10.1007/s00267-011-9625-4

McCallum, J. L., Höhne, A., Schaper, J. L., Shanafield, M., Banks, E. W., Posselt, M., et al. (2020). A numerical stream transport modeling approach including multiple conceptualizations of hyporheic exchange and spatial variability to assess contaminant removal. *Water Resources Research*, *56*(3), e2019WR024987. https://doi.org/10.1029/2019wr024987

Meghdadi, A., & Javar, N. (2018). Evaluation of nitrate sources and the percent contribution of bacterial denitrification in hyporheic zone using isotope fractionation technique and multi-linear regression analysis. *Journal of Environmental Management*, *222*, 54–65. https://doi.org/10.1016/j.jenvman.2018.05.022

Metropolis, N., Rosenbluth, A. W., Rosenbluth, M. N., Teller, A. H., & Teller, E. (1953). Equation of state calculations by fast computing machines. *Journal of Chemical Physics*, *21*(6), 1087–1092. https://doi.org/10.1063/1.1699114

Mohamed, R. A. M., Brooks, S. C., Tsai, C.-H., Ahmed, T., Rucker, D. F., Ulery, A. L., et al. (2021). Geostatistical interpolation of streambed hydrologic attributes with addition of left censored data and anisotropy. *Journal of Hydrology and Hydromechanics*, *599*, 126474. https://doi.org/10.1016/j.jhydrol.2021.126474

Mousavi, S. J., Abbaspour, K. C., Kamali, B., Amini, M., & Yang, H. (2012). Uncertainty-based automatic calibration of HEC-HMS model using sequential uncertainty fitting approach. *Journal of Hydroinformatics*, *14*(2), 286–309. https://doi.org/10.2166/hydro.2011.071

Poeter, E. P., & Hill, M. C. (1999). UCODE, a computer code for universal inverse modeling code. *Computers & Geosciences*, *25*(4), 457–462. https://doi.org/10.1016/S0098-3004(98)00149-6. Retrieved from http://water.usgs.gov/software/ground_water.html1

Raue, A., Kreutz, C., Maiwald, T., Bachmann, J., Schilling, M., Klingmüller, U., & Timmer, J. (2009). Structural and practical identifiability analysis of partially observed dynamical models by exploiting the profile likelihood. *Bioinformatics*, *25*(15), 1923–1929. https://doi.org/10.1093/bioinformatics/btp358

Riscassi, A., Miller, C., & Brooks, S. (2016). Seasonal and flow-driven dynamics of particulate and dissolved mercury and methylmercury in a stream impacted by an industrial mercury source. *Environmental Toxicology and Chemistry*, *35*(6), 1386–1400. https://doi.org/10.1002/etc.3310

Rowiński, P. M., Dysarz, T., Napiorkowski, J. J., Greco, M., Caravetta, A., & Della Morte, R. (2004). *Estimation of longitudinal dispersion and storage zone parameters* (pp. 1201–1210). Taylor & Francis Group.

Rucker, D. F. (2011). Inverse upscaling of hydraulic parameters during constant flux infiltration using borehole radar. *Advances in Water Resources*, *34*(2), 215–226. https://doi.org/10.1016/j.advwatres.2010.11.001

Rucker, D. F., Tsai, C. H., Carroll, K. C., Brooks, S., Pierce, E. M., Ulery, A., & Derolph, C. (2021). Bedrock architecture, soil texture, and hyporheic zone characterization combining electrical resistivity and induced polarization imaging. *Journal of Applied Geophysics*, *188*, 104306. https://doi.org/10.1016/j.jappgeo.2021.104306

Runkel, R. L. (1998a). One-dimensional transport with inflow and storage (OTIS): A solute transport model for streams and rivers. In *Water Resources Investigation Report 98-4018*. U.S. Dep. of the Inter., U.S. Geol. Survey.

Runkel, R. L. (1998b). One-dimensional transport with inflow and storage (OTIS): A solute transport model for streams and rivers. In *USGS Water-Resources Investigation Report, 98-4018* (pp. 1–73).

Runkel, R. L. (2002). A new metric for determining the importance of transient storage. *Journal of the North American Benthological Society*, *21*(4), 529–543. https://doi.org/10.2307/1468428

Scott, D. T., Gooseff, M. N., Bencala, K. E., & Runkel, R. L. (2003). Automated calibration of a stream solute transport model: Implications for interpretation of biogeochemical parameters. *Journal of the North American Benthological Society*, *22*(4), 492–510. https://doi.org/10.2307/1468348

Šimůnek, J., & Hopmans, J. W. (2002). 1.7 parameter optimization and nonlinear fitting. In *Methods of soil analysis* (pp. 139–157).

Stegen, J. C., Johnson, T., Fredrickson, J. K., Wilkins, M. J., Konopka, A. E., Nelson, W. C., et al. (2018). Influences of organic carbon speciation on hyporheic corridor biogeochemistry and microbial ecology. *Nature Communications*, *9*(1), 585. https://doi.org/10.1038/s41467-018-02922-9

Trauth, N., Schmidt, C., Vieweg, M., Maier, U., & Fleckenstein, J. H. (2014). Hyporheic transport and biogeochemical reactions in pool-riffle systems under varying ambient groundwater flow conditions. *Journal of Geophysical Research-Biogeosciences*, *119*(5), 910–928. https://doi.org/10.1002/2013jg002586

U.S. EPA. (1997). Method 300.1: Determination of inorganic anions in drinking water by ion chromatography. Retrieved from https://www.epa.gov/esam/epa-method-3001-revision-10-determination-inorganic-anions-drinking-water-ion-chromatography

Vrugt, J. A., Hopmans, J. W., & Simunek, J. (2001). Calibration of a two-dimensional root water uptake model. *Soil Science Society of America Journal*, *65*(4), 1027–1037. https://doi.org/10.2136/sssaj2001.6541027x

Wagener, T., Camacho, L. A., & Wheater, H. S. (2002). Dynamic identifiability analysis of the transient storage model for solute transport in rivers. *Journal of Hydroinformatics*, *94*(3), 199–211. https://doi.org/10.2166/hydro.2002.0019

Wagner, B. J., & Gorelick, S. M. (1986). A statistical methodology for estimating transport parameters: Theory and applications to one-dimensional advective-dispersive systems. *Water Resources Research*, *22*(8), 1303–1315. https://doi.org/10.1029/wr022i008p01303

Wagner, B. J., & Harvey, J. W. (1997). Experimental design for estimating parameters of rate-limited mass transfer: Analysis of stream tracer studies. *Water Resources Research*, *33*(7), 1731–1741. https://doi.org/10.1029/97wr01067

Wang, L., Goh, M., Ding, R. G., & Pretorius, L. (2019). Improved simulated annealing based risk interaction network model for project risk response decisions. *Decision Support Systems*, *122*, 113062. https://doi.org/10.1016/j.dss.2019.05.002

Ward, A. S., & Packman, A. I. (2019). Advancing our predictive understanding of river corridor exchange. *WIREs Water*, *6*(1), e1327. https://doi.org/10.1002/wat2.1327

Ward, A. S., Wondzell, S. M., Schmadel, N. M., Herzog, S., Zarnetske, J. P., Baranov, V., et al. (2019). Spatial and temporal variation in river corridor exchange across a 5th-order mountain stream network. *Hydrology and Earth System Sciences*, *23*(12), 5199–5225. https://doi.org/10.5194/hess-23-5199-2019

Wlostowski, A. N., Gooseff, M. N., Bowden, W. B., & Wollheim, W. M. (2017). Stream tracer breakthrough curve decomposition into mass fractions: A simple framework to analyze and compare conservative solute transport processes. *Limnology and Oceanography: Methods*, *15*(2), 140–153. https://doi.org/10.1002/lom3.10148

Yeh, T. C., Khaleel, R., & Carroll, K. C. (2015). *Flow through heterogeneous geologic media*. Cambridge University Press.